Materials Research Bulletin 44 (2009) 1586–1591

Contents lists available at ScienceDirect

Materials Research Bulletin

journal homepage: www.elsevier.com/locate/matresbu

Crystal and magnetic structure and cation distribution of $Mn_{2-x}V_{1+x}O_4$ spinels ($x = 0$, 1/3 and 1)

E.V. Pannunzio-Miner [a], J.M. De Paoli [a,b], R.D. Sánchez [b], R.E. Carbonio [a,*]

[a] INFIQC-CONICET, Departamento de Fisicoquímica, Facultad de Ciencias Químicas, Universidad Nacional de Córdoba, 5000 Córdoba, Argentina
[b] Centro Atómico Bariloche, Comisión Nacional de Energía Atómica, 8400 Bariloche, Argentina

ARTICLE INFO

Article history:
Received 27 November 2008
Accepted 29 January 2009
Available online 7 February 2009

Keywords:
A. Oxides
B. Chemical synthesis
C. Neutron scattering
C. X-ray diffraction
D. Magnetic properties

ABSTRACT

We synthesized the spinel-type compounds belonging to the $Mn_{2-x}V_{1+x}O_4$ series with $x = 0$, 1/3 and 1 as polycrystalline powders. Crystal and magnetic structures were refined using synchrotron X-ray and neutron powder diffraction. At 300 K all members crystallize in the cubic system, space group $Fd\bar{3}m$, and show a structural transition at low temperature, changing to a tetragonal symmetry (space group $I4_1/amd$). Cations distributions between octahedral and tetrahedral sites were refined from neutrons diffraction (ND) data and explained based on crystal field stabilization energies (CFSE) and ionic radii. The magnetic unit cell is the same as the crystallographic one, having identical symmetry relations. The magnetic structure was refined as an arrangement of collinear spins, antiferromagnetically ordered, parallel to the *c*-axis of the unit cell. The refined site magnetic moments are smaller than those obtained from hysteresis cycles of the *M* vs. *H* measurements, indicating that some non-collinear disordered component coexists with the ordered component along the *c*-axis.

1. Introduction

Materials belonging to the spinel family have the stoichiometry AB_2X_4, where *A* and *B* are cations of either 2+ and 3+ charge or of 4+ and 2+ charge, and *X* represents O^{2-} or chalcogenides (like S^{2-} and Te^{2-}) [1]. The structure is based on the cubic close-packing of anions with the cations located on 1/8 of the tetrahedral (T) and 1/2 of the octahedral (O) sites. The general formula for the cationic distribution is $(A_{1-\gamma}B_{\gamma})^{T}\,[B_{2-\gamma}\,A_{\gamma}]^{O}O_4$; where γ is the degree of inversion ($0 \leq \gamma \leq 1.0$) and T and O indicate tetrahedral and octahedral sites, respectively. A knowledge of the cation distribution between O and T sites is crucial, since it determines the magnetic and electrical properties of the spinels, thus, the knowledge of this distribution is important in controlling and predicting the physical properties of spinels [2,3]. Neutrons diffraction (ND) can give an unambiguous picture of this distribution, since usually neutron coherent scattering lengths significantly differ for the different cations, consequently ND is essential in studying cations distribution in spinels.

Since the magnetoresistance effect (MR) was discovered in spinel-type compounds [4,5] these have been the subject of renewed studies in the field of material sciences. Although their MR is not as marked as that of some perovskites, spinel-type materials are attractive candidates for MR materials because a great number of spinels have ferrimagnetic properties and display some kind of electrical conductivity. Consequently, the search for magnetic spinels which might present MR effect is of technological importance.

The magnetic unit cell of the spinels usually is the same as the crystallographic one, having identical symmetry relations [6,7] and when both cations are magnetic, the magnetic moments of the B and A sites are antiferromagnetically ordered. An important characteristic of the spinel oxides is that it is possible to vary the ionic composition without significant structural changes, to tune, enhance, or modify physical properties.

Spinel oxides of V constitute an interesting class of compounds as they exhibit a wide variety of electronic properties, depending on the V–V distance [8]. As d_{V-V} decreases, there is a change from an antiferromagnetic insulator to a paramagnetic metallic compound; MnV_2O_4 was classified in the insulator side [8].

As we were interested in ferrimagnetic spinels which potentially could display some MR effects, we prepared and characterized the structural and magnetic properties of spinel-type oxides $Mn_{2-x}V_{1+x}O_4$ with $x = 0$, 1/3 and 1.

One of the end members ($x = 1$) MnV_2O_4 was synthesized before [9–20] and some of its structural and magnetic properties have been studied [10,12–20]. The magnetic structure was first elucidated by Plumier and Sougi [12]. Recently, a detailed study

* Corresponding author. Tel.: +54 351 433 4180/4169; fax: +54 351 433 4188.
E-mail address: carbonio@mail.fcq.unc.edu.ar (R.E. Carbonio).

0025-5408/$ – see front matter © 2009 Elsevier Ltd. All rights reserved.
doi:10.1016/j.materresbull.2009.01.022

performed by using single crystal neutron diffraction measurements, has been published [13]. They refine the magnetic structure with the Mn (Mn^{2+}) magnetic moments aligned parallel to the tetragonal *c* axes and the V (V^{3+}) magnetic moments with components on any of the three axes but with *a* and *b*-axes components constrained to form an orthogonally stacked AFM structure. However, the cation distribution has not been specifically refined.

The other end member ($x = 0$) Mn_2VO_4 has been synthesized as well but no data other than the unit cell dimensions were reported [21]. In order to better characterize the $Mn_{2-x}V_{1+x}O_4$ series and explore the possibility of finding an MR effect, we synthesized again the two end-members ($x = 0$ and $x = 1$), and an intermediate member with $x = 1/3$. This last composition was selected since, if we assume that Mn is in the 2+ oxidation state, half of the V would be in the 4+ oxidation state and half in the 3+ oxidation state. Since Mn and V are very close in the periodic table, we use ND in order to better determine cations distributions between O and T sites and to refine the magnetic structure. The neutrons scattering lengths for Mn and V (3.9, −0.50) are much more different between them than the corresponding X-rays scattering factors, so that it is possible to refine with confidence their occupation factors using ND.

2. Experimental

These compounds were synthesized from mixtures of MnO, V_2O_3 and VO_2, in ratios corresponding to the stoichiometry of the desired phase. Powdered reagents were ground and mixed using an agate mortar, pressed into pellets and heated in evacuated sealed silica tubes at 1273 K. Two heating cycles of 12 h separated by regrinding, were necessary to achieve a low content of impurities, as evaluated by laboratory X-ray diffraction. Besides, for the sample with $x = 1$ (MnV_2O_4) an additional heat treatment of 12 hs in an atmosphere of H_2(5%):Ar(95%) was necessary in order to stabilize V^{3+} and to reduce the amount of impurities, otherwise relatively large amounts of them were present. Laboratory XRD measurements were done in the 2θ range 10.0–100.0° with an angular step of 0.02° using Cu Kα radiation in a Philips X'Pert Pro Diffractometer. Reaction products were also examined using a scanning electron microscope (SEM) equipped with an energy-dispersive (EDS) detector.

Symmetry and unit cell dimensions were determined using high-resolution synchrotron X-ray powder diffraction (SXRPD) patterns measured at 300 and 20 K at the D10A diffractometer in the Laboratorio Nacional de Luz Sincrotron (LNLS), Campinas, Brazil ($\lambda = 1.61019$ Å) in the 2θ range 15.0–100.0° with an angular step of 0.01°. Crystal structure, cation site occupancies and magnetic structure were refined using neutron diffraction patterns ($\lambda = 1.5945$ Å) obtained at 300 and 4 K at the D2B line in the Laüe Langevin Institute (Grenoble, France) in the 2θ range 5.0–160.0° with an angular step of 0.01°.

The FULLPROF program [22] was used to refine the crystal structure by the Rietveld method. A pseudo-Voigt shape function was always adequate to obtain good fits for NPD and SXRPD. All RT diffraction data were refined in the cubic space group $Fd\bar{3}m$ and low temperature data were refined in the tetragonal space group $I4_1/amd$. The following parameters were refined for the NPD data: scale factor, zero-point error, unit-cell parameters, pseudo-Voigt corrected for asymmetry parameters, positional coordinates, isotropic thermal factors and occupation factors of Mn/V. The coherent scattering lengths for Mn, V and O were 3.9, −0.50 and 5.80 fm, respectively. The refined parameters for the SXRPD data were: scale factor, zero-point error, unit-cell parameters, pseudo-Voigt corrected for asymmetry parameters, positional coordinates and isotropic thermal factors.

DC magnetization was measured with a commercial superconducting quantum interference device magnetometer on powdered samples, with a maximum magnetic field of 10 kOe and in the 5–300 K temperature (*T*) range.

3. Results

3.1. SEM images and EDS analysis

The sample with $x = 1/3$ is composed of crystals dominated by the form {1 1 1} (i.e., octahedrons), as can be seen in SEM images (Fig. 1). Crystals are often found in parallel growths, and some may display twinning. Samples with $x = 0$ and $x = 1$, are composed of aggregates of grains with no evident crystalline faces. No cations other than Mn and V were detected in the reaction products using EDS (results not shown).

3.2. Crystal and magnetic structure

3.2.1. Crystal structure and cations distributions

SXRPD data taken at room temperature were refined in the cubic $Fd\bar{3}m$ space group (Fig. 2a) (only refined diffractograms for $x = 1$ are shown). At low temperatures (20 K) most of the reflections are split, indicating a lowering of symmetry (as an example, see in the inset of Fig. 2 the region of [3 1 1]). We could fit these data with the tetragonal $I4_1/amd$ model (Fig. 2b). Crystallographic parameters for the spinel compounds $Mn_{2-x}V_{1+x}O_4$ refined from SXRPD data are shown in Table 1 for all compositions. At $T = 20$ K, these phases have a slight tetragonal distortion, which could be measured by $d = (c/a)2^{1/2}$; $d = 1$ indicates a cubic phase. Although these values are very close to 1, the tetragonal distortion is clearly seen by the splitting of the reflections (Fig. 2c). This transition from cubic to tetragonal system was observed in the $x = 1$ composition by Suzuki et al. at $T = 53$ K [17] and Garlea et al. [13] and it was assigned to orbital

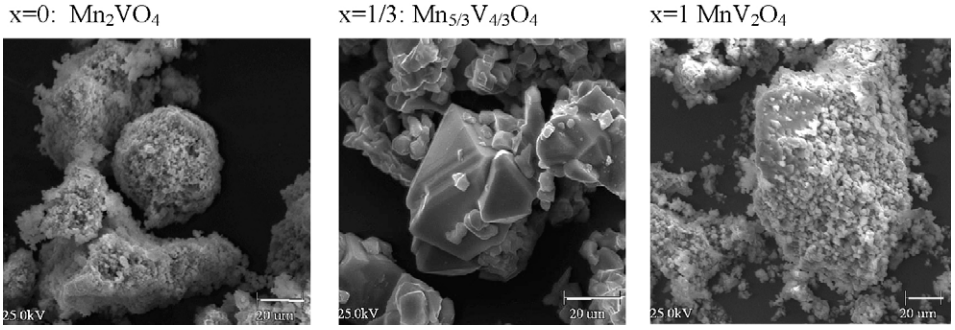

Fig. 1. SEM images of $Mn_{2-x}V_{1+x}O_4$ ($x = 0$, 1/3 and 1) polycrystalline samples.

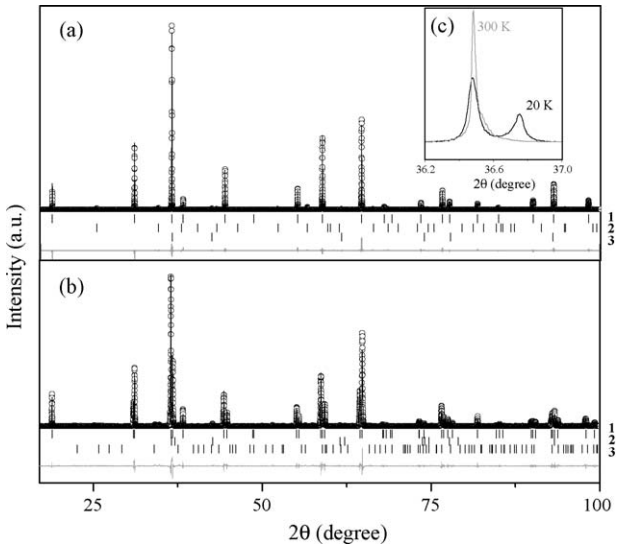

Fig. 2. Refined synchrotron X-ray powder diffraction pattern for MnV_2O_4 at (a) 300 K (*Fd* $\bar{3}$*m*) and (b) 20 K (*I*4$_1$/*amd*). Observed (circles), calculated (solid line) and difference (solid line at the bottom). The vertical lines correspond to the positions of Bragg reflections (1 = spinel, 2 = MnO (2%) and 3 = V_2O_3 (2%)). Inset: Zoomed pattern in the 3 1 1 zone (for the cubic indexing) showing cubic to tetragonal phase transition.

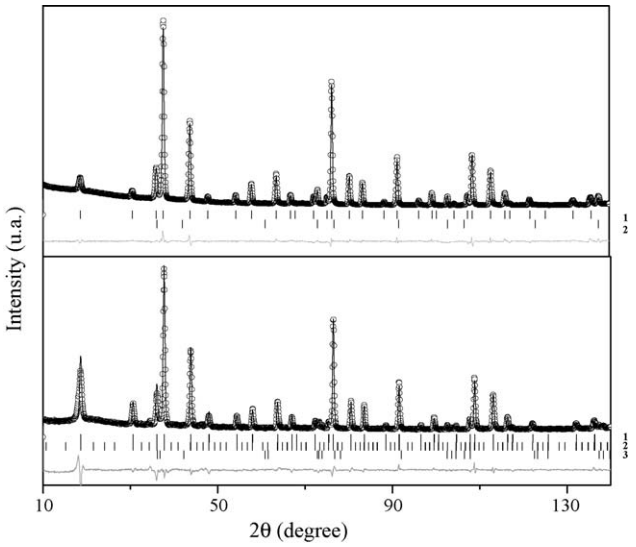

Fig. 3. Refined Neutron powder diffraction pattern for $Mn_{5/3}V_{4/3}O_4$ (x = 1/3) at (a) 300 K (*Fd* $\bar{3}$*m*) and (b) 4 K (*I*4$_1$/*amd*). Observed (circles), calculated (solid line) and difference (solid line at the bottom). The vertical lines correspond to the positions of Bragg reflections (1 = spinel, 2 = MnO and 3 = spinel magnetic phase).

Table 1
Lattice parameters refined from Rietveld analysis of synchrotron X-ray powder diffraction data for $Mn_{2-x}V_{1+x}O_4$ (x = 0, 1/3 and 1) spinels at 300 and 20 K.

x	Compound	300 K *Fd* $\bar{3}$*m*	20 K *I*4$_1$/*amd*		
		a (Å)	a (Å)	c (Å)	d
0	Mn_2VO_4	8.5276(2)	6.0485(2)	8.5669(2)	1.0015
1/3	$Mn_{5/3}V_{4/3}O_4$	8.5617(1)	6.0421(2)	8.5472(2)	1.0003
1	MnV_2O_4	8.5771(2)	6.0417(1)	8.4427(2)	0.9881

ordering [13,17,23–25]. SXRPD was only used to refine cell parameters and to clearly show the tetragonal distortion at low temperatures. Since the X-ray scattering factor (f) for O is too low and $f_{Mn} \approx f_V$ it is not possible to obtain accurate values of O atomic positions and cation occupancies. For these reasons, in order to obtain a rigorous description of the structure, we use ND.

The refined ND pattern at RT is presented in Fig. 3 (only x = 1/3 is shown). The occupancies of the cations (Wyckoff sites 8*a* and 16*d* for the cubic ones and 4a and 8d for the tetragonal ones) were refined in such a way that the whole stoichiometry was maintained. During the refinements, cell parameters were fixed to their values obtained by SXRPD and the neutrons wavelength was refined (the variations in the neutron wavelength during refinement was in the third decimal figure). Refined O positions, occupancies and isotropic temperature factors are shown in Table 2. For the cubic phases the oxygen position *32e* (u, u, u) is described conventionally by u-parameter. For our phases, u-parameter lies within its normal limit of 0.240–0.275 for the spinel structure [26]. The cell parameter decreases as x increases from 0 to 1. This is in agreement with the Shannon and Prewitt's ionic radii for cations in sixfold coordination: $r(Mn^{2+})$ = 0.83 Å, $r(Mn^{3+})$ = 0.645 Å, $r(V^{4+})$ = 0.58 Å and $r(V^{3+})$ = 0.64 Å and fourfold coordination: $r(Mn^{2+})$ = 0.66 Å [27].

Refined ND data at 4K are shown in Fig. 3 (only data for the x = 1/3 compound is shown). Refined parameters and agreement factors are listed in Table 2. Selected bond distances and angles are listed in Table 3. We allowed occupancies to vary during refinements with respect to their values at RT. The observed differences are within the experimental errors. The refined occupancies at 300 K, thus, allow us to write the following formulas:

$$x = 0 (Mn_2VO_4): \quad (Mn_{0.89}V_{0.11})^{T}(Mn_{1.11}V_{0.89})^{O}O_4$$
$$x = \frac{1}{3}(Mn_{5/3}V_{4/3}O_4): \quad (Mn_{1.00})^{T}(Mn_{0.67}V_{1.33})^{O}O_4$$
$$x = 1 (MnV_2O_4): \quad (Mn_{0.75}V_{0.25})^{T}(Mn_{0.25}V_{1.75})^{O}O_4$$

Even though MnV_2O_4 has been extensively studied before [9–20], all the authors have assumed that this spinel was a normal one, however, our results indicate that, at least for powdered samples prepared with our synthetic method, there is a quite large degree of inversion (γ = 0.25).

With our NPD experiments we are able to deduce what the elemental distribution among the sites is, but we are unable to univocally assign oxidation states. In order to elaborate a model for this distribution we will take into account thermodynamic considerations. Cation distribution in spinels containing transition metals can usually be correlated to crystal field stabilization energies (CFSE) and cation radii of transition metal ions in octahedral and tetrahedral environments [28]. In our compounds there is a clear preference of V for the O sites, this can be attributed to crystal field effects. In principle, the possible oxidation states for V are V^{3+} and V^{4+} (there are no V^{2+} spinel oxides found in literature and V^{5+} is too oxidized for our synthetic reducing conditions) and those for Mn are Mn^{2+} and Mn^{3+} (Mn^{4+} is too oxidized for our synthetic reducing conditions). Assuming that octahedral field stabilization energy (Δ_O) and tetrahedral field stabilization energy (Δ_T) are correlated through $\Delta_T \approx 4/9\Delta_O$ [29], we can estimate the CFSE of all the ions (See Table 4). Clearly V^{3+} and Mn^{3+} have larger preference for O sites than for T sites. Mn^{2+} has no CFSE, but according to O'Neill and Navrotsky in 2–3 spinels, larger cations have preference for T sites [28].

If we assume that Mn is only present as Mn^{2+} and according to the previous comments, then the predicted cations distribution is (Model I):

$$x = 0 (Mn_2VO_4): \quad (Mn_{0.89}{}^{2+}V_{0.11}{}^{4+})^{T}[Mn_{1.11}{}^{2+}V_{0.89}{}^{4+}]^{O}O_4$$
$$x = \frac{1}{3}(Mn_{5/3}V_{4/3}O_4): \quad (Mn_{1.00}{}^{2+})^{T}[Mn_{0.67}{}^{2+}V_{0.66}{}^{3+}V_{0.67}{}^{4+}]^{O}O_4$$
$$x = 1 (MnV_2O_4): \quad (Mn_{0.75}{}^{2+}V_{0.25}{}^{3+})^{T}[Mn_{0.25}{}^{2+}V_{1.75}{}^{3+}]^{O}O_4$$

Table 2
Structural parameters, refined from Rietveld analysis of neutron powder diffraction patterns and calculated magnetic moments for $Mn_{2-x}V_{1+x}O_4$ (x = 0, 1/3 and 1) spinels at 300 and 5 K.

300 K			4 K				
Site/atom	B_{iso}	Occ	Site/atom	B_{iso}	Occ	μ (μ_{bohr})	$\mu_{theoretical}$ (μ_{bohr})
x = 0 $(Mn_{0.89}V_{0.11})^T(Mn_{1.11}V_{0.89})^OO_4$, γ = 0.444							
8a Mn1	1.241(7)	0.037(1)	*4a* Mn1	0.750(2)	0.111(2)	2.57(2)	4.56(2)
8a V1		0.005(1)	*4a* V1		0.014(2)		
16d Mn2	1.75(1)	0.046(2)	*8d* Mn2	1.921(8)	0.139(2)	−0.87(1)	−3.22(2)
16d V2		0.037(2)	*8d* V2		0.112(2)		
32e O	2.61(3)	0.1667	*16h* O	2.441(3)	0.500	–	–
32*e* site, u = 0.26223(2), R_{wp} = 11.4, R_{Bragg} = 5.6, χ^2 = 3.2			*16h* site, x = 0, y = 0.4845(1), z = 0.2677(8), R_{wp} = 12.6, R_{Bragg} = 4.7, χ^2 = 2.26				
x = 1/3 $(Mn)^T(Mn_{0.69}V_{1.31})^OO_4$, γ = 0.00							
8a Mn1	0.816(3)	0.042(1)	*4a* Mn1	0.667(2)	0.125(2)	3.14(2)	5.92(2)
8a V1		0.000(1)	*4a* V1		0.000(2)		
16d Mn2	0.829(2)	0.028(1)	*8d* Mn2	0.471(2)	0.085(2)	−2.38(2)	−2.49(3)
16d V2		0.055(1)	*8d* V2		0.165(2)		
32e O	1.636(1)	0.1667	*16h* O	0.993(3)	0.500	–	–
32*e* site, u = 0.2626(1), R_{wp} = 10.1, R_{Bragg} = 3.8, χ^2 = 2.6			*16h* site, x = 0, y = 0.4790(9), z = 0.2664(5), R_{wp} = 7.84, R_{Bragg} = 4.9, χ^2 = 3.01				
x = 1 $(Mn_{0.75}V_{0.25})^T(Mn_{0.26}V_{1.74})^OO_4$, γ = 0.127							
8a Mn1	0.614(8)	0.031(3)	*4a* Mn1	0.187(2)	0.122(1)	1.72(2)	4.08(3)
8a V1		0.011(2)	*4a* V1		0.003(1)		
16d Mn2	1.192(2)	0.011(2)	*8d* Mn2	0.554(1)	0.007(2)	−0.62(2)	−1.87(3)
16d V2		0.073(3)	*8d* V2		0.243(2)		
32e O	1.441(2)	0.1667	*16h* O	1.202(2)	0.500	–	–
32e site, u = 0.2641, R_{wp} = 12.9, R_{Bragg} = 4.4, χ^2 = 2.1			*16h* site, x = 0, y = 0.4740, z = 0.2644, R_{wp} = 15.5, R_{Bragg} = 5.1, χ^2 = 2.7				

Table 3
Selected bond distances (Å) and angles (°) for $Mn_{2-x}V_{1+x}O_4$ (x = 0, 1/3 and 1) spinels determined by Rietveld analysis of neutron powder diffraction patterns at 300 and 5 K.

Temperature	Distances (Å)			Angles (°)		
	(Mn_1/V_1)–O	(Mn_2/V_2)–O	(Mn_2/V_2)–(Mn_2/V_2)	O–(Mn_1/V_1)–O	O–(Mn_2/V_2)–O	(Mn_2/V_2)–(Mn_2/V_2)–(Mn_2/V_2)
x = 0, Mn_2VO_4						
300 K	4*x* 2.03886(5)	6*x* 2.04462(5)	3*x* 3.03247(8)	109.471(4)	3*x* 83.968(3) 3*x* 96.032(4)	60.0
4 K	4*x* 2.0321(5)	2*x* 1.9813(8) 4*x* 2.0737(7)	2*x* 3.0266 (3) 1*x* 3.0243(2)	2*x* 105.427(3) 4*x* 111.53(5)	2*x* 96.14(5) *c*-axis 2*x* 86.06(3) 2*x* 93.94(6)	2*x* 60.025 (4) 1*x* 59.950(2)
x = 1/3, $Mn_{5/3}V_{4/3}O_4$						
300 K	4*x* 2.03983(3)	6*x* 2.03871(3)	3*x* 3.02711(5)	109.471(3)	3*x* 83.806(2) 3*x* 96.194(2)	60.0
4 K	4*x* 2.0357(5)	2*x* 1.9981(8) 4*x* 2.0540(5)	2*x* 3.02141(3) 1*x* 3.02094(4)	2*x* 106.98(2) 4*x* 110.73(5)	2*x* 96.62(4) *c*-axis 2*x* 84.74(2) 2*x* 95.26(5)	1*x* 59.990(1) 2*x* 60.005(1)
x = 1, MnV_2O_4						
300 K	4*x* 2.05461(4)	6*x* 2.01890(4)	3*x* 3.01506(5)	109.471(3)	3*x* 82.979(3) 3*x* 97.021(3)	60.0
4 K	4*x* 2.0412(4)	2*x* 1.9953(7) 4*x* 2.0317(4)	2*x* 3.00305(3) 1*x* 3.02086(8)	2*x* 109.56(3) 4*x* 109.43(2)	2*x* 96.79(4) *c*-axis 2*x* 83.54(2) 2*x* 96.46(4)	1*x* 60.393(2) 2*x* 59.804(2)

If the reduction of V^{4+} caused by oxidation of Mn^{2+} to Mn^{3+} is considered (in an extreme case where all the V^{4+} is reduced to V^{3+}), then 2–3 type spinels can be generated (this is only possible for the x = 0 and x = 1/3 compounds since x = 1 already has all V as V^{3+}). If this would be the case, the thermodynamically favored arrangements would be (Model II):

From the bond distances $(Mn_1/V_1)_{(4a)}$–O (for T sites) and $(Mn_2/V_2)_{(8d)}$–O (for O sites) and the angles O–(Mn_1/V_1)–O (for T sites) and O–(Mn_2/V_2)–O (for O sites) in the low temperature phase we can deduce the nature of the distortions in these polyhedra (see Table 3). Flattening or elongation of tetrahedra or octahedral in spinels is usually associated to Jahn–Teller distortions [24,31–33].

$$x = 0 (Mn_2VO_4): \quad (Mn_{0.89}{}^{2+}V_{0.11}{}^{3+})^T[Mn_{1.00}{}^{3+}Mn_{0.11}{}^{2+}V_{0.89}{}^{3+}]^OO_4$$

$$x = \frac{1}{3}(Mn_{5/3}V_{4/3}O_4): \quad (Mn_{1.00}{}^{2+})^T[Mn_{0.67}{}^{3+}V_{1.33}{}^{3+}]^OO_4$$

$$x = 1 (MnV_2O_4): \quad (Mn_{0.75}{}^{2+}V_{0.25}{}^{3+})^T[Mn_{0.25}{}^{2+}V_{1.75}{}^{3+}]^OO_4 \text{ (this is the same as in model I)}$$

Table 4
Crystal field stabilization energies calculated for octahedral (O) and tetrahedral (T) occupied by Mn and V ions in $Mn_{2-x}V_{1+x}O_4$ ($x = 0$, 1/3 and 1) spinels.

Ion	$(CFSE)^O$	$(CFSE)^T$	$(CFSE)^O-(CFSE)^T$
V^{4+}	$0.4\Delta_o$	$0.27\Delta_o$	$0.13\Delta_o$
V^{3+}	$0.8\Delta_o$	$0.53\Delta_o$	$0.27\Delta_o$
Mn^{3+}	$0.6\Delta_o$	$0.18\Delta_o$	$0.42\Delta_o$
Mn^{2+}	$0.0\Delta_o$	$0.0\Delta_o$	$0.0\Delta_o$

In our case for all the compounds there is a small compression of the octahedral. However, there is an elongation of the tetrahedra (four angles larger than 109.4° and two shorter) for the $x = 0$ and 1/3 compounds, resulting in extremely small tetragonal distortions (see values of d in Table 1) and a compression of the tetrahedra for the $x = 1$ compound, resulting in a tetragonal distortion a little bit larger ($d = 0.9882$). Because of these very small distortions of the polyhedra we have not enough evidence to associate them with Jahn–Teller distortions.

3.2.2. Magnetic structure

At 4 K, the low angle reflections in the NDP patterns increase significantly (Fig. 3b). We assume that these contributions are entirely of magnetic origin. In most of the oxo-spinels with paramagnetic ions at the T and O sites, the crystallographic and magnetic unit cells are the same, having identical symmetry relations [6,7], therefore lower angle Bragg peaks are masked with magnetic contributions. However, Plumier and Sougui [12], found that the $x = 1$ composition, MnV_2O_4, has two-ordered magnetic structures. One of them, present in a narrow interval between 56 and 54 K, displaying an antiparallel and collinear order between magnetic moments in the A and B sites. Below 52 K, however, the structure was found to present a 63° canting of the magnetic moments in the B site, whose resultant moment is opposite to the magnetic moment of the A site. This arrangement was called a triangular structure. Between 54 and 52 K a mixed triangular and paramagnetic phase was found. Canting can be detected mainly due to the appearance of the 0 0 2 reflection (following the tetragonal cell indexing). In our case, this reflection is completely absent in all the NDP, so we can discard the existence of this triangular phase at 4 K. Consequently we propose as the starting model of the magnetic structure an arrangement of collinear spins, antiferromagnetically ordered, parallel to the c-axis of the unit cell. Thus, the full pattern was refined simultaneously with two models, one to account for the crystallographic structure and another one to account for the magnetic structure. Starting values of the O and T site moments were set according to values calculated using the free ion saturation moments and the refined cation occupancies and later they were refined. Table 2 shows the results of refinements and also a comparison of the calculated and observed site magnetic moments. An antiferromagnetic coupling is evident between the magnetic moments of the O and T sites. Our refined site magnetic moments are smaller that the calculated ones. This indicates that some non-collinear disordered component coexists with the ordered component along the c-axis. Since non-collinear spins are randomly oriented, they do not contribute to the Bragg peaks, thus resulting in reduced ordered moments.

Recently, Garlea et al. [13], using single crystal neutron diffraction, refined the magnetic structure of MnV_2O_4 with the Mn (Mn^{2+}) magnetic moments aligned parallel to the tetragonal c axes and the V (V^{3+}) magnetic moments with components on any of the three axes but with a and b-axes components constrained to form an orthogonally stacked AFM structure. We use the magnetic structure they propose to calculate a theoretical diffractogram. The results are shown in Fig. 4 (we show only results for $x = 1$, for other samples we obtain similar ones). It is clear from the comparison

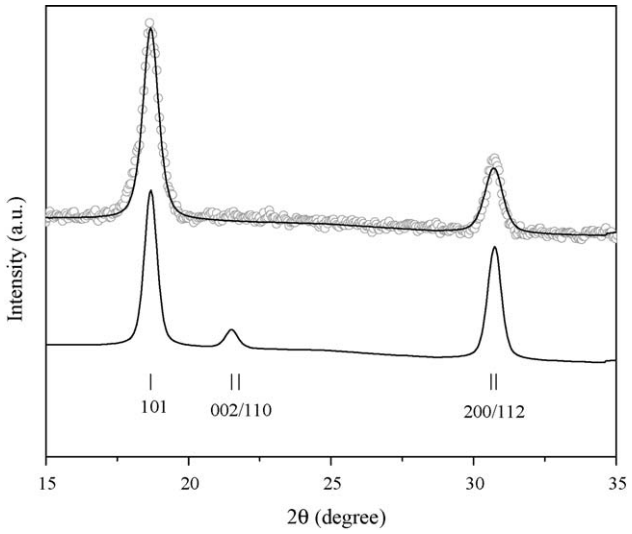

Fig. 4. Zoomed region of the ND powder diffractogram between 15° and 35° for MnV_2O_4 showing a comparison between experimental (circles), refined with collinear magnetic moments (on top of experimental points) and calculated with model proposed in Ref. [13] (at the bottom).

that the model proposed by Garlea et al. is not adequate for our samples. The magnetic reflection 0 0 2/1 1 0 is absent, the 2 0 0/1 1 2 is larger and the 1 0 1 smaller.

3.2.3. Magnetic measurements

For all composition, the magnetic field (H) dependence of magnetization (M) at 5 K are depicted in Fig. 5. All the hysteresis loops show high coercive field values (between 1 and 2 kOe), indicating that some important magnetic anisotropy is present in the system. On the other hand, at high magnetic field the saturation magnetization values (n^M_B) are 0.9, 0.8 and 1.1 μ_B/mol for the $x = 0$, 1/3 and 1 compositions respectively (see Table 5). It is interesting to compare these values with those (n^N_B) obtained from the Rietveld refinement of the magnetic structure using neutron diffraction data, which are 1.33, 0.83 and 2.08 μ_B/mol for $x = 0$, 1/3 and 1. Note that the n^N_B values are always higher than n^M_B. This is reasonable, since by ND we obtain the real magnetic moment in each site which is ordered, constituting a periodic arrangement, on the other side, by using the magnetization measurements, we measure a macroscopic average, which will be coincident in the "ideal" limiting case were we obtain a single

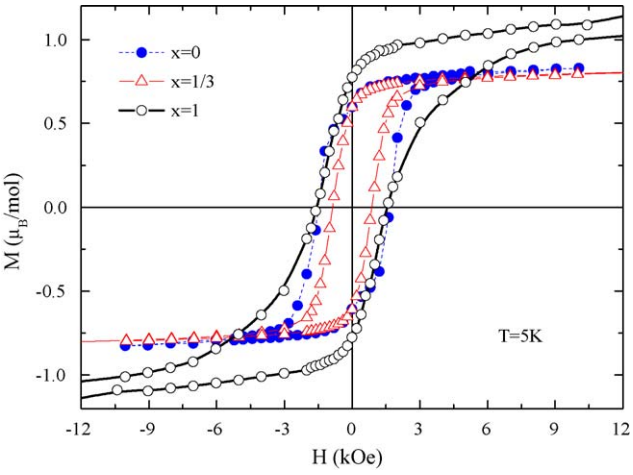

Fig. 5. Magnetization vs. magnetic field at $T = 5$ K for $Mn_{2-x}V_{1+x}O_4$.

Table 5
Saturation magnetization values obtained from: NPD refinements (n^N_B); magnetization vs. H hysteresis loops (n^M_B) and calculated from the ionic models (n_B) for $Mn_{2-x}V_xO_4$ spinels.

	n^N_B (μ_B) Neutron exp.	n^M_B (μ_B) Magnetization exp.	n_B (μ_B) Calculated	
			Model I	Model II
$x = 0$, Mn_2VO_4	1.33	0.9	1.88	1.66
$x = 1/3$, $Mn_{5/3}V_{4/3}O_4$	0.83	0.8	0.34	0.34
$x = 1$, MnV_2O_4	2.08	1.1	0.50	0.50

magnetic domain. This will be experimentally accessed only at very large H values and at very low temperatures. Actually, our results for the x = 0 and 1 samples are in good agreement with those informed in literature [see Table XVI in ref. 34].

Now, we principally focus our attention to find any explanation about these values using the proposed models. Taking into account that (i) the electronic spin configurations present in the more feasible models are Mn^{2+}, Mn^{3+}, V^{3+} and V^{4+} are $3d^5$, $3d^4$, $3d^2$ and $3d^1$, respectively; (ii) the saturation moments expected for each of these chemical species are 5 μ_B, 4 μ_B, 2 μ_B and 1 μ_B per mol of ions; (iii) our recent knowledge about A and B ions occupancies (which has been mentioned in the precedent paragraphs) and (iv) that $J_{AB} > J_{BB} > J_{AA}$ (which is expected for the spinels); we can calculate assuming Néel order between the A and B sub-lattices using $n_B = M_B - M_A$ formula. The results are shown in Table 5. The differences observed between the experimental results and the different ideal ionic models proposed could arise for a variety of reasons. The principal reason could be some disordered component or some intra-site exchange constant.

We will continue the discussion of the possible models based on additional magnetic and electrical measurements in another publication [30].

4. Conclusions

Crystal and magnetic structures of the $Mn_{2-x}V_{1+x}O_4$ compounds were refined using synchrotron X-ray and neutron diffraction. At 300 K all members crystallize in the cubic system, space group $Fd\bar{3}m$, and show a structural transition at low temperature, changing to a tetragonal symmetry (space group $I4_1/amd$). Cations distributions were refined from ND data. Using these refinements and thermodynamic considerations we propose for $x = 0$ (Mn_2VO_4) the crystallographic formula: $(Mn^{2+}_{0.89}V^{3+}_{0.11})^T[Mn^{3+}_{1.00}Mn^{2+}_{0.11}V^{3+}_{0.89}]^OO_4$; for $x = 1/3$ ($Mn_{5/3}V_{4/3}O_4$): $(Mn^{2+}_{1.00})^T[Mn^{2+}_{0.67}V^{3+}_{0.66}V^{4+}_{0.67}]^OO_4$ and for $x = 1$ (MnV_2O_4): $(Mn^{2+}_{0.75}V^{3+}_{0.25})^T[Mn^{2+}_{0.25}V^{3+}_{1.75}]^OO_4$. These cations distribution was explained according to site preferences based on CFSE and ionic radii. The magnetic structure was refined as an arrangement of collinear spins, antiferromagnetically ordered, parallel to the c-axis of the same unit cell as the crystallographic one. M vs. H experiments give hysteresis loops with high coercive field values (between 1 and 2 kOe), indicating that some important magnetic anisotropy is present in the system. The saturation magnetization values (n^M_B) were 0.9, 0.8 and 1.1 μ_B/mol for the $x = 0$, 1/3 and 1 compositions, respectively. The n^N_B values were always higher than n^M_B, this is reasonable, since by ND we obtain the real magnetic moment in each site which is ordered, constituting a periodic arrangement, on the other side, by using the magnetization measurements, we measure a macroscopic average, which will be coincident in the "ideal" limiting case were we obtain a single magnetic domain.

There was a large discrepancy between the calculated site magnetic moments using the ideal ionic models and those obtained either from NPD or from magnetic measurements, the principal reason for this could be some disordered component or some intra-site exchange constant.

Acknowledgments

R.E.C. and R.D.S. thank ANPCYT (Projects PAV 22708, PICT 06-15102 and 21372) and CONICET (PIP 5767/05 and 5250/05). R.E.C. also thanks SECyT-UNC (Project 197/05). R.D.S. also thanks SEPCyT-UNCu. E.V.P.M. and J.M.D. thank CONICET for a fellowship. We thank LNLS (Campinas, Brazil) for access to D10A powder diffractometer and ILL (Grenoble, France) for access to D2B line.

References

[1] Hk. Müller-Buschbaum, J. Alloys Compd. 349 (2003) 49–104.
[2] S.M. Yunus, H. Yamauchi, A.K.M. Zakaria, N. Igawa, A. Hoshikawa, Y. Haga, Y. Ishii, J. Alloys Compd. 455 (2008) 98–105.
[3] B.E. Martin, A. Petric, J. Phys. Chem. Solids 68 (2007) 2262–2270.
[4] A.P. Ramirez, R.J. Cava, J. Krajewski, Nature 386 (1997) 156–159.
[5] J. Philipp, T.R.N. Kutty, Mater. Lett. 39 (1999) 311–317.
[6] S.M. Yunus, H. Yamauchi, A.K.M. Zakaria, N. Igawa, A. Hoshikawa, Y. Ishii, J. Alloys Compd. 454 (2008) 10–15.
[7] A.K.M. Zakaria, M.A. Asgar, S.G. Eriksson, F.U. Ahmed, S.M. Yunus, A.K. Azad, Physica B 385–386 (2006) 106–109.
[8] S. Blanco-Canosa, F. Rivadulla, V. Pardo, D. Baldomir, J.-S. Zhou, M. García Hernández, M.A. López Quintela, J. Rivas, J.B. Goodenough, Phys. Rev. Lett. 99 (2007) 187201.
[9] B. Reuter, E. Riedel, P. Hug, D. Arndt, U. Geisler, J. Behnke, Z. Anorg. Allg. Chem. 369 (1969) 306.
[10] J.C. Bernier, P. Poix, Ann. Chim. Paris (1967) 81–85.
[11] K. Adachi, T. Suzuki, K. Kato, K. Osaka, M. Takata, T. Katsufuji, Phys. Rev. Lett. 95 (2005) 197202–197205.
[12] (a) R. Plumier, M. Sougi, Physica B 155 (1989) 315–319;
(b) R. Plumier, M. Sougi, Solid State Commun. 64 (1987) 53–55.
[13] V.O. Garlea, R. Jin, D. Mandrus, B. Roessli, Q. Huang, M. Miller, A.J. Schultz, S.E. Nagler, Phys. Rev. Lett. 100 (2008) 66404–66407.
[14] V. Hardy, Y. Béard, C. Martin, Phys. Rev. B 78 (2008) 24406–24413.
[15] S.-H. Baek, K.-Y. Choi, A.P. Reyes, P.L. Kuhns, N.J. Curro, V. Ramanchandran, N.S. Dalal, H.D. Zhou, C.R. Wiebe, J. Phys. Condens. Matter 20 (2008) 135218–135224.
[16] T. Kstsufuji, K. Adachi, T. Suzuki, M. Katsumura, Physica B 383 (2006) 13–15.
[17] T. Suzuki, M. Katsumura, K. Taiguchi, T. Arima, T. Katsufuji, Phys. Rev. Lett. 98 (2007) 127203–127206.
[18] K. Miyoshi, M. Ihara, K. Fujiwara, J. Takeuchi, Physica B 281–282 (2000) 30–31.
[19] Y. Hu, Y.-H. Liu, Mater. Chem. Phys. 90 (2005) 255–261.
[20] T. Sonehara, K. Kato, K. Osaka, M. Takata, T. Katsufuji, Phys. Rev. B 74 (2006) 104424–104430.
[21] J.C. Bernier, P. Poix, A. Michel, Mem. Soc. Chim. Paris (1963) 1724–1728.
[22] J. Rodríguez-Carbajal, Physica B 192 (1993) 55–57.
[23] Y. Motome, H. Tsunetsugu, Physica B 359 (2005) 1222–1224.
[24] P. Radaelli, New J. Phys. 7 (2005) 53–74.
[25] (a) T. Suzuki, M. Katsumura, K. Taniguchi, T. Arima, T. Katsufuji, Phys. Rev. Lett. 98 (2007) 127203–127207;
(b) S. Di Mateo, G. Jackeli, N.B. Perkins, Phys. Rev. B 72 (2005) 20408–20412;
(c) O. Tchernyshyov, Phys. Rev. Lett. 93 (2004) 157206–157209.
[26] P. Roderick, R.J. Hill, J.R. Craig, G.V. Gibbs, Phys. Chem. Miner. 4 (1979) 317–339.
[27] R.D. Shannon, Acta Cryst. A 32 (1976) 751–767.
[28] (a) H.St.C. O'Neill, A. Navrotsky, Am. Mineral. 68 (1983) 181–194;
(b) H.St.C. O'Neill, A. Navrotsky, Am. Mineral. 69 (1984) 733–753.
[29] J.D. Dunitz, L.E. Orgel, J. Phys. Chem. Solids 3 (1957) 318–323.
[30] E.V. Pannunzio-Miner, J.M. De Paoli, R.E. Carbonio, R.D. Sánchez, J. Appl. Phys., in press.
[31] B.J. Kennedy, Q. Zhou, J. Solid State Chem. 181 (2008) 2227–2230.
[32] M. Tovar, R. Torabi, C. Welker, F. Fleischer, Physica B 385–386 (2006) 196–198.
[33] L. Ortega San Martín, A.J. Williams, C.D. Gordon, S. Klemme, J.P. Attfield, J. Phys.: Condens. Matter 20 (2008) 104238–104242.
[34] J.B. Goodenough, Magnetism and the Chemical Bond, John Wiley and Sons, 1963